Remote origins of interannual variability in the Indonesian Throughflow region from data and a global Parallel Ocean Program simulation

Julie L. McClean¹ and Detelina P. Ivanova¹ Department of Oceanography, Naval Postgraduate School, Monterey, California, USA

Janet Sprintall

Scripps Institution of Oceanography, University of California, San Diego, La Jolla, California, USA

Received 10 May 2004; revised 31 May 2005; accepted 6 July 2005; published 14 October 2005.

[1] The mean and interannual variability of the thermal structure of the World Ocean Circulation Experiment (WOCE) repeat IX1-expendable bathythermograph (XBT) transect between Java and Western Australia were compared statistically for the years 1987–1997 with concurrent, co-located output from a global eddy-permitting configuration of the Parallel Ocean Program (POP) model forced with realistic surface fluxes. Dominant variability at long timescales for both model and data in the southern IX1 region was associated with Pacific El Niño-Southern Oscillation (ENSO) events; at the northern end it was due to remote equatorial Indian Ocean forcing and Indian Ocean Dipole Mode events. In the Indo-Pacific domain the model reproduced the structure and magnitude of observed low-frequency variability. Event analyses following the warm ENSO phase showed low-frequency off-equatorial Rossby waves interacting with the North Pacific western maritime boundary to reflect onto the equator and excite a coastally trapped response that propagated through the Indonesian seas and along the northwest coast of Australia. In turn, the signal progressively propagated away from this coast as free baroclinic Rossby waves to 90°E. Cross-spectral analyses confirmed that on interannual timescales, both off-equatorial and equatorial signals remotely forced in the Pacific were largely responsible for the strong observed and modeled variability at the southern end of IX1.

Citation: McClean, J. L., D. P. Ivanova, and J. Sprintall (2005), Remote origins of interannual variability in the Indonesian Throughflow region from data and a global Parallel Ocean Program simulation, J. Geophys. Res., 110, C10013, doi:10.1029/2004JC002477.

Introduction

[2] The Indonesian Seas form an oceanic conduit of momentum, heat, and freshwater between the Pacific and Indian oceans that significantly impacts the thermohaline balance of both basins [Bryden and Imawaki, 2001; Wijffels et al., 2001]. Much effort has been expended to understand both the magnitude and variability of these fluxes (see Lukas et al. [1996], Godfrey [1996], and Gordon [2001] for reviews). Remote forcing from both the Pacific and Indian ocean basins, as well as the regional monsoon forcing, complicates the property flux estimates within the Indonesian seas, causing variability over a range of timescales.

[3] A particularly significant data set that has contributed to our understanding of the Indonesian Throughflow (ITF) variability is the expendable bathythermograph (XBT)

San Diego, La Jolla, California, USA.

Niño-Southern Oscillation (ENSO). Second mode variability was associated with a modulation of the annual cycle off Java, due to reversals in the South Java Current [Quadfasel and Cresswell, 1992; Sprintall et al., 1999]. Correlations between the amplitude time series of the first joint EOF mode and the zonal wind stress in the Pacific and Indian oceans revealed a maximum correlation in the western central Pacific, with secondary maximums occurring over the equatorial Indian and eastern Pacific oceans. Drawing on the findings of Clarke and Liu [1994], M96 attributed these results to a remote Pacific signal comprised of energy from equatorial Rossby waves passing the New Guinea-Australia landmass and equatorial Kelvin waves

measurements collected along the IX1 transect between Java and northwest Australia since 1983 [Mevers et al.,

1995; Meyers, 1996] (the latter hereinafter referred to as

M96). M96 state that this data set is representative of the

ITF on long timescales; hence it has provided a means of

monitoring interannual variability of the Throughflow. An

empirical orthogonal function (EOF) analysis of this data

revealed the dominant variability to be associated with El

C10013 1 of 18

¹Now at Scripps Institution of Oceanography, University of California,

reflected from the Indonesia/Borneo/Asia boundary that was transmitted along the northwest (NW) coast of Australia, and Indian Ocean equatorial Kelvin waves propagating along the eastern Indian Ocean boundary.

- [4] In a very recent paper, Wijffels and Meyers [2004] used lagged partial regression analyses to relate the interannual temperature and sea level variability in the Indonesia seas and the southern Indian Ocean to remote winds along the equator of the Indian and Pacific oceans. Much of the response was explained by these equatorial winds that produced free equatorial Kelvin and Rossby waves whose signals reached the study region. Equatorial Pacific Rossby waves excited coastally trapped waves off the western tip of New Guinea that propagated poleward along the Arafura/ Australian shelf break. As well, Pacific energy radiated westward into the southeast Indian Ocean via the Banda Sea. Equatorial Indian Ocean Kelvin waves penetrated as far as the Savu Sea, the western Banda Sea, and Makassar Strait. As in M96, their findings further substantiate those of Clarke and Liu [1994], who first identified this region as one where two oceanic waveguides intersect.
- [5] Long period, off-equatorial baroclinic Rossby waves have recently been documented in the Pacific basin by White et al. [2003]. Biennial (2.2- and 2.8-year), interannual (3.5-, 5.4-, and 7-year), and decadal (11-year) Rossby waves propagate westward across the Pacific basin to reach the western boundary at approximately 7°N, 12°N, and 18°N, respectively. The waves form in response to off-equatorial cyclonic wind stress curl anomalies, induced by westerly surface wind anomalies produced in the wake of warm sea surface temperature (SST) anomalies that propagate slowly eastward along the equator. On reaching the western maritime boundary of the Pacific, these waves excite coastallytrapped Munk-Kelvin waves, identified by Godfrey [1975] and further explained by McCreary [1983], that propagate southwards to reflect back onto the equator as equatorial Kelvin waves [Pazan et al., 1986; White et al., 1989]. White et al. [2003] report the reflected signals as slow equatorial coupled waves, producing a delayed negative feedback to the warm SST anomalies located in the central Pacific. This process represents a modification of the delayed action oscillation El Niño model [Philander, 1990] such that in addition to the equatorial Rossby waves that reflect as equatorial Kelvin waves, feedback is provided by offequatorial biennial, interannual, and decadal Rossby waves. White et al. [2003] used the NCEP/NCAR reanalysis and the Scripps Institution of Oceanography (SIO) upper ocean temperature reanalysis data sets to identify the Pacific waves. In this paper we use a global ocean general circulation model (OGCM), whose grid spacing and realistic topography resolve the waveguide through the Indonesian Seas, to determine if these off-equatorial low-frequency signals, once reflected back onto the equator, excite coastally trapped signals that propagate through the Indonesian Seas and along the northwest coast of Australia. White et al. [2003] did not consider this pathway in their analyses. M96 and Wijffels and Meyers [2004] only considered the equatorial Pacific Rossby waves that generate coastally trapped waves with pathways through the Indonesian seas.
- [6] The transmission of coastally trapped signals through the Indonesian passages has been documented using numerical models of varying complexity. *Wajsowicz* [1996]

performed a suite of sensitivity runs using a 1° × 1° OGCM containing simplified, idealized or realistic, complex representations of the Indonesian archipelago within the largescale Pacific-Indian domain. She identified coastal Kelvin waves on the west Australian coast emerging from the idealized Indonesian archipelago. These coastally trapped waves resulted when off-equatorial Rossby waves generated by negative wind stress curl in the North Pacific reached the western boundary of the Pacific and were partially scattered into the archipelago and partially reflected into the equatorial waveguide. Potemra [1999], using a 1-1/2 layer reduced gravity model forced with monthly climatological winds, reported that annual winds just north of the equator in the eastern Pacific produced annual Rossby waves by Ekman pumping. These off-equatorial waves interacted with the western boundary of the Pacific to form coastal Kelvin waves that propagated through the Indonesian Seas. Schiller et al. [2000] found that both the IX1 data and output from a coarse resolution OGCM forced with interannual fluxes revealed a shallower (deeper) thermocline associated with the arrival of El Niño (La Niña) signals along the west Australian coast at the southern end of the section. They attributed the upwelling (downwelling) to the passage of Kelvin waves originating from the tip of Irian-Jaya. Using a 0.5° grid model driven by ERS satellite winds, Masumoto [2002] found two dominant modes in the model surface dynamic height on interannual timescales, corresponding to ENSO Pacific forcing and eastern Indian Ocean forcing, that confirm the observations of M96 and Wijffels and Meyers [2004]. However, in agreement with Yamagata et al. [1996], Masumoto [2002] suggested that variations in the model Throughflow transport have highest correlation with the second mode's Indian Ocean variability.

[7] In this paper, we perform some of the same analyses as in M96, but include more recently collected data and use the 1987–1997 period, when sampling along the IX1-XBT transect was increased to be near fortnightly. The variability at the location of the IX1 transect is analyzed using a global eddy-permitting (1/3°, 32 vertical levels) configuration of the Parallel Ocean Program (POP) model forced with daily European Center for Medium Range Forecasts (ECMWF) wind stresses, heat and freshwater fluxes for 1979–1997. The decade-long time series of XBT data provides us with a means of evaluating the ability of the model to reproduce interannual variability in the Subtropical Indian Ocean (STIO). We then use the model to explore forcing mechanisms that are not possible from data alone. Particularly, we provide support for our hypothesis that some of the coastally trapped wave signals that propagate through the Indonesian Seas and along the NW Australian shelf are excited by equatorial Kelvin waves resulting from Kelvin-Munk wave reflection that in turn were excited by off-equatorial baroclinic Rossby waves on reaching the western boundary of the North Pacific Ocean. This wave process at interannual timescales is in addition to the equatorial Pacific signal that radiates through the ITF and into the STIO as discussed by Clarke and Liu [1994], M96, and Wijffels and Meyers [2004]. The model will also be used to understand the impact of remotely forced signals from the Indian and Pacific Oceans on the eastern STIO. The propagation of variability from the eastern boundary into the Indian Ocean could substantially impact the coupled ocean-atmosphere

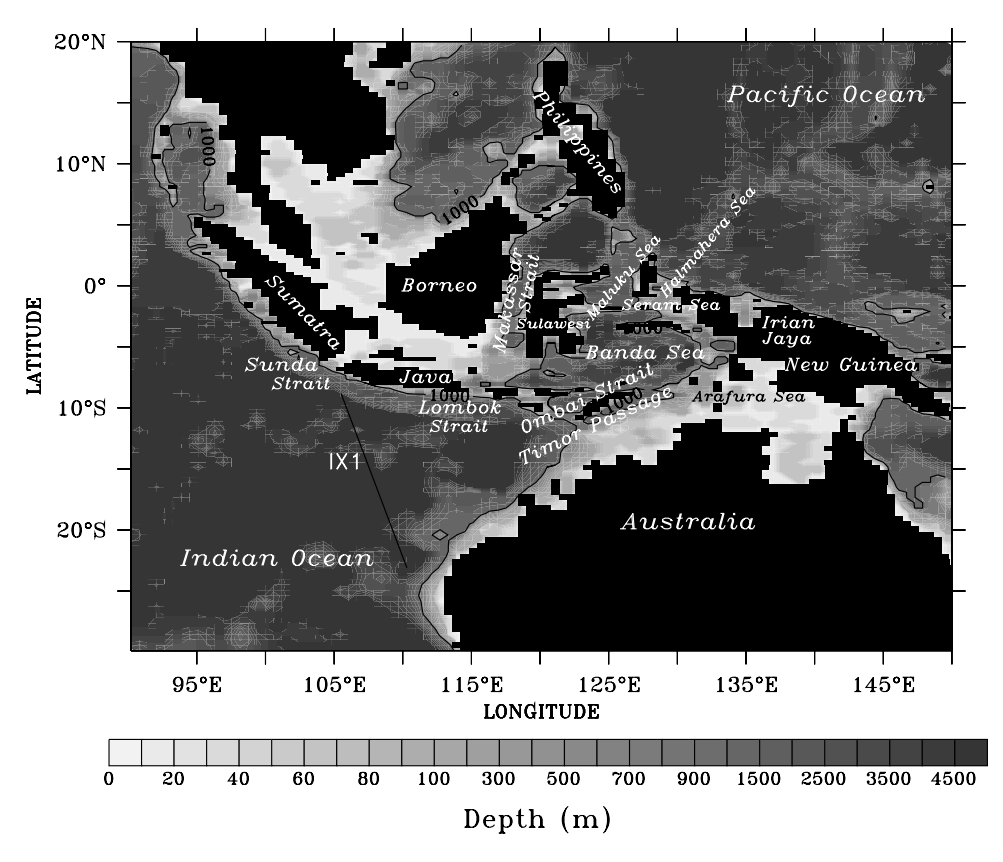


Figure 1. Bathymetry of the Indonesian Seas, the western tropical Pacific, and the southeastern Indian Ocean from *Smith and Sandwell* [1997] topography interpolated onto the 1/3°, 32-level global POP grid. The thick black line between Java and Australia identifies the repeat XBT line known as WOCE IX1. The 1000-m isobath is contoured in black.

system [Morrow and Birol, 1998] and affect SST variability in the STIO [Behera et al., 2000; Murtugudde et al., 2000; Xie et al., 2002]. In the study presented here, we will use a combination of statistical and event analyses, using both model and data, to examine the role of remotely forced interannual variability within the STIO. It is anticipated that coupled climate models will be run using eddy-permitting ocean models in the near future. Before this occurs however, we need to understand the representation of low-frequency variability in stand-alone ocean models at this resolution to simulate modes of variability such as those on interannual time-scales, in the tropics and elsewhere.

[8] The paper is organized in the following manner: details of the in situ data are provided in section 2 while the model is described in section 3. Results of the comparative analyses of the observed and modeled thermal structure in the waters between Java and Australia are found in section 4, while section 5 contains a discussion of the nature of the remote signals influencing this region in the model. Conclusions are found in section 6.

2. Data

[9] A repeat XBT-line between Fremantle, Western Australia, and Sunda Strait, at the western end of Java (Figure 1), was designated IX1 in 1983 as part of the Tropical Ocean-Global Atmosphere (TOGA) XBT network, and continued during the World Ocean Circulation Experiment (WOCE).

The sampling frequency was increased from 6 sections per year in 1983-1986, to >18 sections per year after 1987, with ~ 100 km spacing between profiles. In this paper, we use the temperature data only from 1987 through 1997, to take advantage of the higher sampling frequency and thus minimize the need for interpolation due to missing data. The density of the XBT sampling can be found in Figure 2 of M96; it shows thorough coverage for 1987-1994 between 7.5° S and 24° S.

[10] To study the Throughflow variability, the 288 available IX1 temperature sections between 1987–1997 were interpolated in time and space. The XBT profile data were first averaged into 10-m vertical bins between 5 and 750 m depth. Monthly means were then calculated. Next, averages were constructed for overlapping bi-months, i.e., January–February, February–March, etc. These fields were then averaged into 1°-latitude bins along the IX1-XBT track between 8°S and 24°S. Finally, optimal interpolation was used to fill in missing values. Dynamic height relative to 400 db was calculated from the temperature observations and a temperature-salinity relationship derived from the raw observer data compiled by *Levitus et al.* [1994a, 1994b] supplemented by more recent WOCE hydrographic data in the region [*Sprintall et al.*, 2002].

3. Global Ocean Model

[11] The ocean model used in this study is the Los Alamos National Laboratory (LANL) Parallel Ocean Pro-

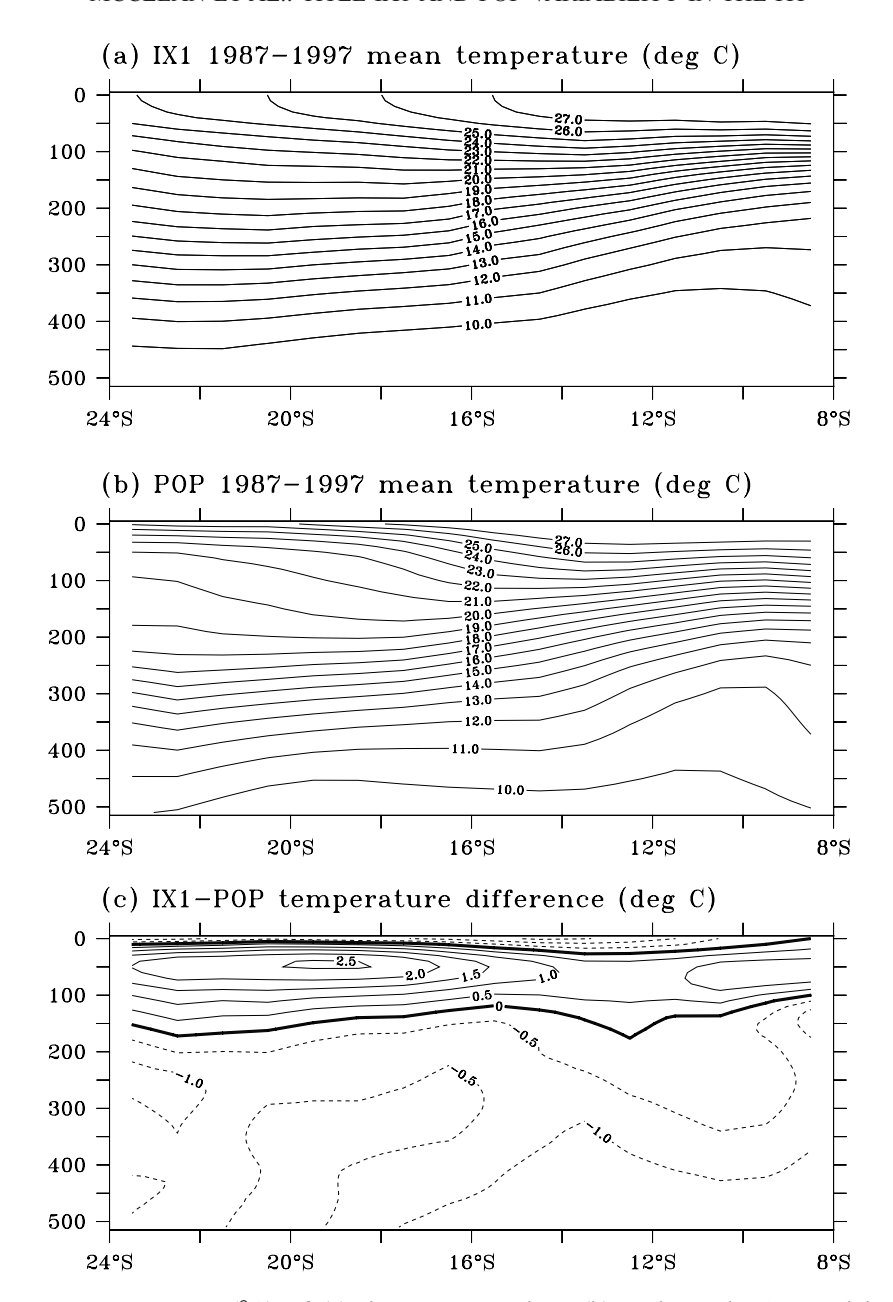


Figure 2. Mean temperature (°C) of (a) the IX1-XBT data; (b) co-located POP model output; and (c) the difference field (°C) between the data and model for 1987–1997.

gram (POP) [Dukowicz and Smith, 1994]. It is a threedimensional, z-level primitive equation ocean general circulation model. The domain is fully global and is configured on a displaced pole grid whereby the North Pole is rotated into Hudson Bay to avoid a polar singularity. The grid is eddy-permitting: it has an average resolution of 1/3° latitude and longitude with increased latitudinal resolution near the equator of about 1/4°, and 32 levels. It was configured to have exactly double the horizontal resolution of the 2/3° global POP used in the Parallel Climate Model (PCM) [Washington et al., 2000], a global coupled air/ ocean/ice/land system used for centennial climate simulations. It is anticipated that the 1/3° POP or some very similarly configured eddy-permitting global POP model will be used in the next-generation higher resolution coupled climate system. A blended global bathymetry was created from the work of *Smith and Sandwell* [1997], with ETOPO5 used in the Antarctic and Arctic. All important sills and channels were checked and modified to encourage correct flow. Figure 1 shows the model bathymetry of the region to be discussed in this paper: the Indonesian Seas and the eastern Indian and western Pacific oceans. The model resolves all the major straits in the Indonesian Seas such as the Makassar, Halmahera, Lombok, Ombai, and Sunda Straits, and Timor Passage. Torres Strait between Australia and New Guinea has been restricted to mimic the very small amount of flow that enters the Arafura Sea directly from the South Pacific.

[12] The model was initialized from the annual *Levitus et al.* [1994a, 1994b] climatology of potential temperature (θ) and salinity (S), and was spun up for 30 years. During the spin-up it was forced with a daily climatology of momen-

tum, heat, and freshwater fluxes formed from 1979-1993 ECMWF daily reanalysis (ERA15) fields. River discharge was included in the daily freshwater fluxes. Daily river runoff values were obtained from annual data [Perry et al., 1996] by dividing the discharge by the number of days in a year, and then distributing over several ocean grid points adjacent to the location of the river mouths. To ensure a global balance of the resulting freshwater and heat fluxes on an annual basis, any globally integrated imbalance for a particular year was equally distributed over that year and over the tropics (20°S to 20°N). This spatial distribution was necessary because of cloud parameterization limitations that would likely significantly impact the tropical regions. Jakob [1999] identified cloud cover deficiencies in the tropics and subtropics by comparing monthly values from the International Satellite Cloud Climatology Project (ISCCP) with the ERA15 fields. To limit model drift, upper level (top 25 m) properties were restored to Levitus et al. [1994a, 1994b] monthly climatological θ and S with a timescale of 6 months.

[13] Biharmonic diffusion operators with spatially varying viscosities and diffusivities are used in POP to perform the horizontal mixing of momentum and tracers. The momentum and tracer coefficients were -0.4×10^{17} cm⁴/s and -0.5×10^{16} cm⁴/s, respectively. They were scaled by $(GCA/GCA_{\min})^2$ where GCA is either the tracer or velocity grid cell area. This choice was made so that mixing would be reduced at progressively higher latitudes. The resulting viscosities and diffusivities are consistent with those used in other eddy-permitting basin-scale numerical studies [Böning and Budich, 1992]. The model time step was 27 min. The Large et al. [1994] mixed layer K-Profile Parameterization (KPP) was turned on at the end of the fifth year of the spin-up.

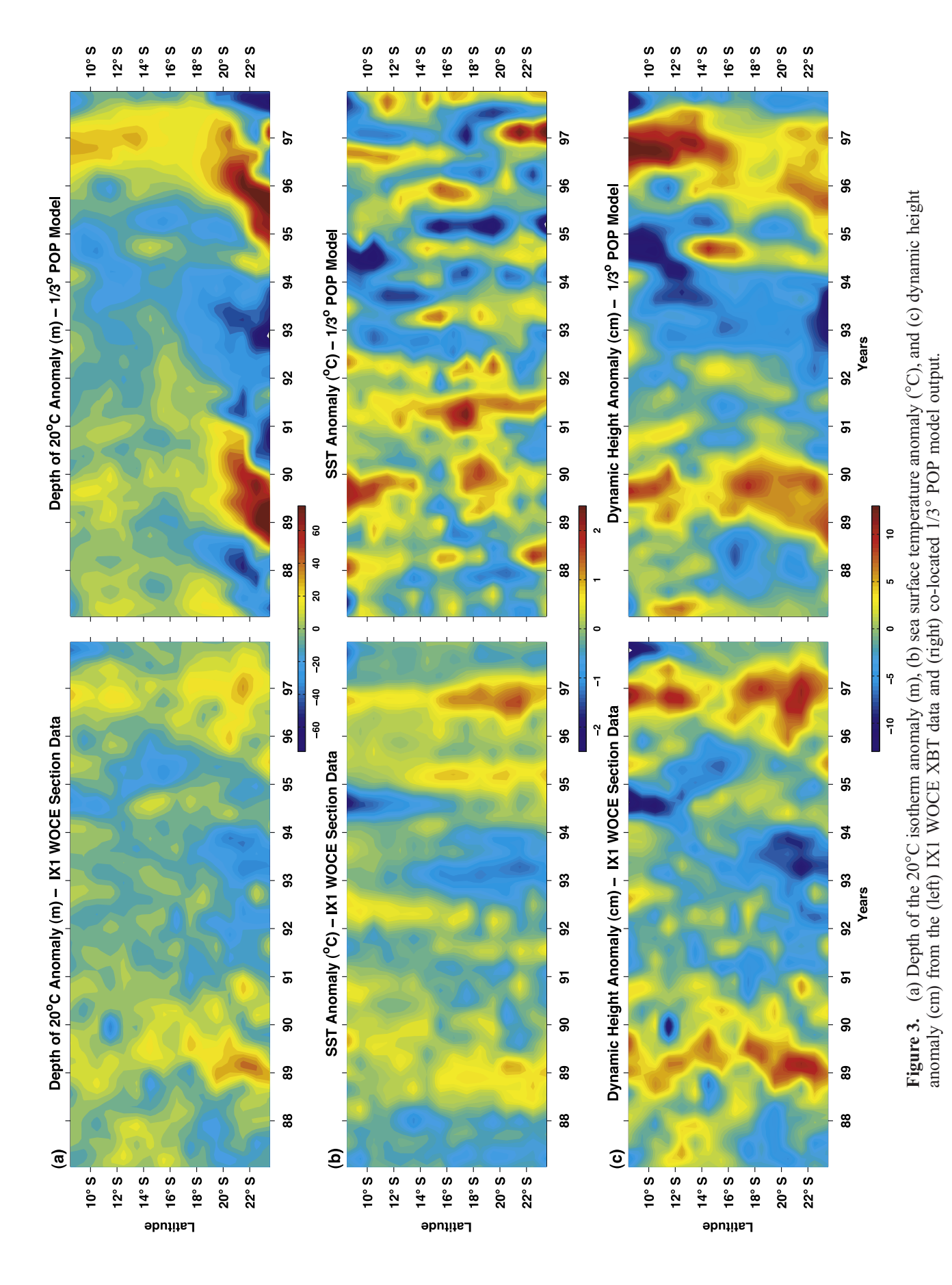
[14] Following the 30-year spin-up, the model was forced with the daily surfaces fluxes formed from the ECMWF reanalysis fields for 1979-1993 and from the ECMWF operational products for 1994-1997. During the 1979-1997 run, 3-day averages of sea surface height, threedimensional meridional and zonal velocity, θ , and S were archived. In order to compare the model output with the IX1 data for 1987-1997, it was necessary to place the model fields on a spatially and temporally co-located grid with the data. Bilinear interpolation was used to extract profiles of simulated θ and S at the station locations from the 3-day model averages that most closely matched the collection dates of the IX1 profiles. The model profiles were then interpolated into the vertical 10-m data grid by means of a cubic spline. The model θ and S were binned horizontally and averaged temporally to the same space and time grid as undertaken for the XBT temperature data. Finally, dynamic height relative to 400 db was calculated using the model temperature and salinity.

4. Results

[15] How well does the POP ocean model reproduce the observed interannual variability in the Indonesian Throughflow region? The frequency and decade-long time series of repeated sampling of the IX1 line allows us to evaluate the model's ability to reproduce the thermal structure on these timescales. However, it is constructive to first examine the

mean temperature fields from the observations (Figure 2a) and the model (Figure 2b), and to understand their differences (Figure 2c). As expected, the observed mean IX1 temperature (Figure 2a) is largely consistent with the earlier study of Meyers et al. [1995]. Against the Java coast, temperature gradients above the thermocline are relatively weak, supporting the idea that the isopycnal signature of the South Java Current (SJC) is dominated by salinity [Wijffels et al., 2002]. Below the thermocline however, at \sim 400 m depth, the dipping of the isotherms reflects the eastward flowing South Java Undercurrent [Sprintall et al., 2002]. Over most of the IX1 transect the thermocline slopes upwards from Australia to Java, indicative of the South Equatorial Current (SEC) and the Indonesian Throughflow waters. Farther south at $\sim 20^{\circ}$ S, eastward shear near the surface indicates the Eastern Gyral Current (EGC): an extension of the southern Indian Ocean subtropical gyre into the region between Australia and Indonesia. Qualitatively, the model (Figure 2b) does a good job in capturing the salient features of the mean observed temperature section. The eastward shear in the South Java Undercurrent is evident, and for the most part the model thermocline also slopes upward toward Java thus successfully capturing the SEC and Throughflow features. South of 16°S, the model has stronger eastward shear between 50 and 200 m, resulting in cooler water relative to the observed (Figure 2c). In the surface layer, model temperature is warmer than the observed. This may be due to a number of causes: inaccuracies in the surface forcing, the use of surface restoring to Levitus et al. [1994a, 1994b] monthly climatology, the lack of tidal mixing in the model, the misrepresentation of isopycnal mixing processes that occurs in z-level models, or a surface flow bias advecting too much warm surface water into the region. Ffield and Gordon [1996] attributed high SST variability at monthly periodicities to tidal mixing in the vicinity of the middle of the IX1 line; lower SSTs result when colder deeper water mixes with that at the surface. This artificially warm surface water may also be responsible for the intensification and trapping of the westward flow in the subsurface south of 17°S.

[16] Following the same approach as M96, we calculated observed and simulated anomaly fields of dynamic height relative to 400 db, SST, and depth of the 20° isotherm (D₂₀) (Figure 3). The anomalies were obtained for both the data and the model by removing the means shown in Figures 2a and 2b, removing the annual and semi-annual cycles by least squares fitting, detrending, and low-pass filtering at 5 months. The interannual signals depicted in the data and model D₂₀, SST, and dynamic height anomaly fields represent a combination of forcing from both the Indian and Pacific oceans. At the southern end of the IX1 transect, the 1987–1997 data show that the 20°C isotherm (Figure 3a) was shallower, SST was cooler (Figure 3b), and dynamic height lower (Figure 3c) during 1991-1995 when the Southern Oscillation Index (SOI) was negative for an extended period. Cooler SSTs and shallow D20 also occurred during the 1986-1987 El Niño event. Warmer SSTs, deeper D₂₀ and elevated dynamic height are evident following the onset of the subsequent 1988–1989 La Niña, and again during 1996 when the SOI was positive. Following this event, D₂₀ started to shoal after the Pacific entered the 1997-1998 El Niño. North of 12°S, the



6 of 18

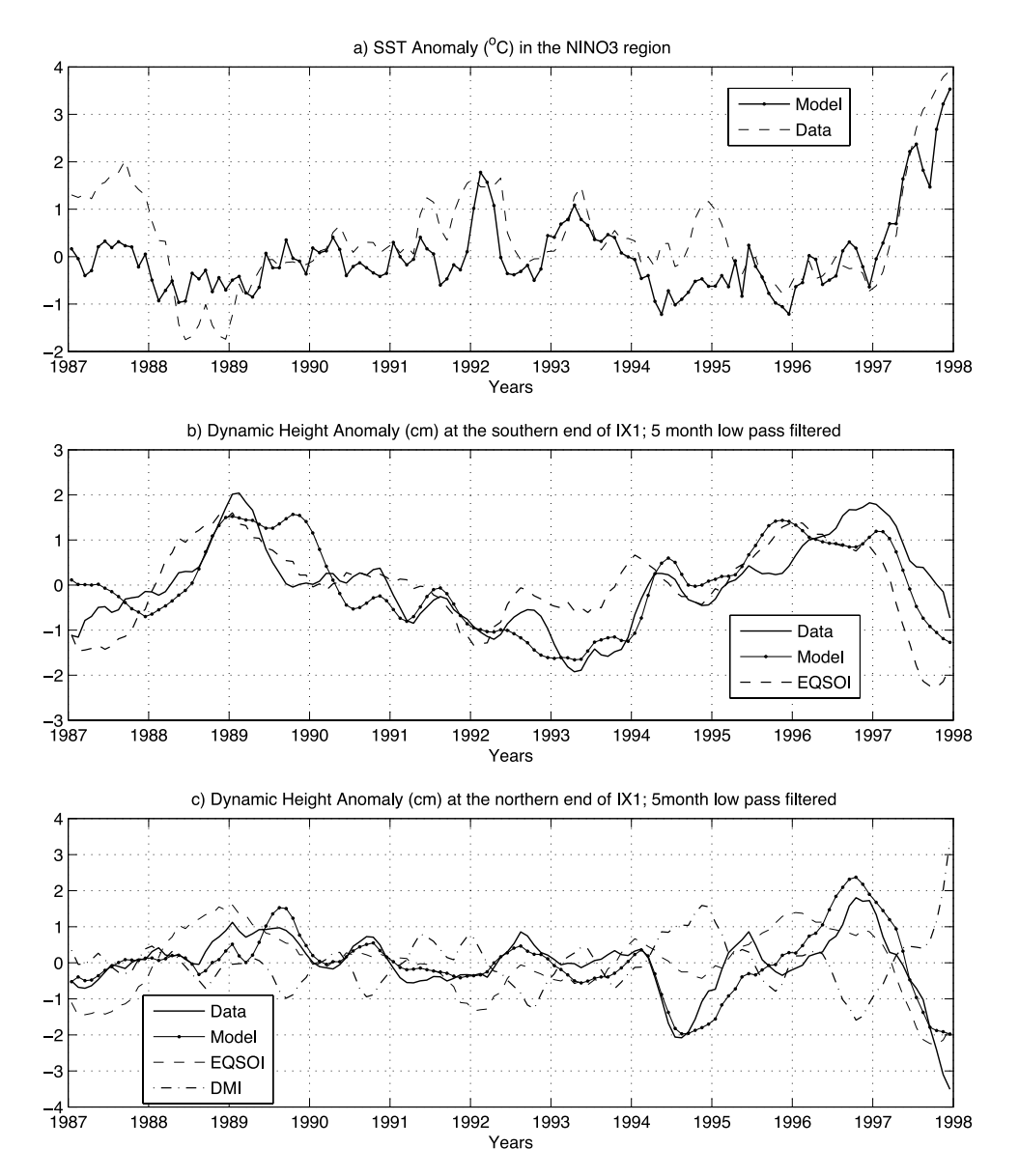


Figure 4. (a) Time series of NINO3 (SSTA for 90°W–150°W, 5°N–5°S) from the model and data [*Reynolds and Smith*, 1994]. Time series of dynamic height anomalies (cm) from (b) southern and (c) northern IX1 calculated from the IX1 XBT data (solid line) and the POP model (solid line with dots). The dashed line is the equatorial Southern Oscillation Index (EQSOI [*Kistler et al.*, 2001]), and the dash-dotted line is the Indian Ocean Dipole Mode Index (DMI [*Saji et al.*, 1999]).

extreme Indian Ocean Dipole (IOD) mode events of 1994 and 1997 are readily identifiable by the cold SST anomalies (Figure 3b) and the lower dynamic height (Figure 3c). In the years prior to these dipole events, warm SST anomalies are observed at the northern end of the section. Saji et al. [1999] have previously documented these events and the biennial tendency in SST for this region. For the period of overlap (1987–1994) as well as the more recent data, our results are in close agreement with M96: Interannual variability in thermocline depth and SST are greatest at the southern end of the IX1 transect and nearly in phase with the Pacific El Niño and La Niña signals, while interannual variability in SST anomalies is large at the northern end of the transect, and closely related to the Indian Ocean dipole mode events.

- [17] Good agreement between the model and data in terms of the spatial and temporal distribution of the anomalies are found in the dynamic height and D_{20} anomaly fields (Figures 3a and 3c). The sequence of simulated dynamic height and D_{20} anomaly events related to El Niño and La Niña track closely with the observed events, however the magnitude of the model anomalies are larger than observed and the duration of the simulated events are too long, particularly for the La Niña event of 1988–1989. The model SST shows the best agreement with data at the section's northern end (Figure 3b).
- [18] Before discussing the influence of the remote ENSO Pacific signal in the STIO, we first examine the veracity of the model ENSO signal itself. We chose to compare the model NINO3 index (monthly SST anomalies averaged

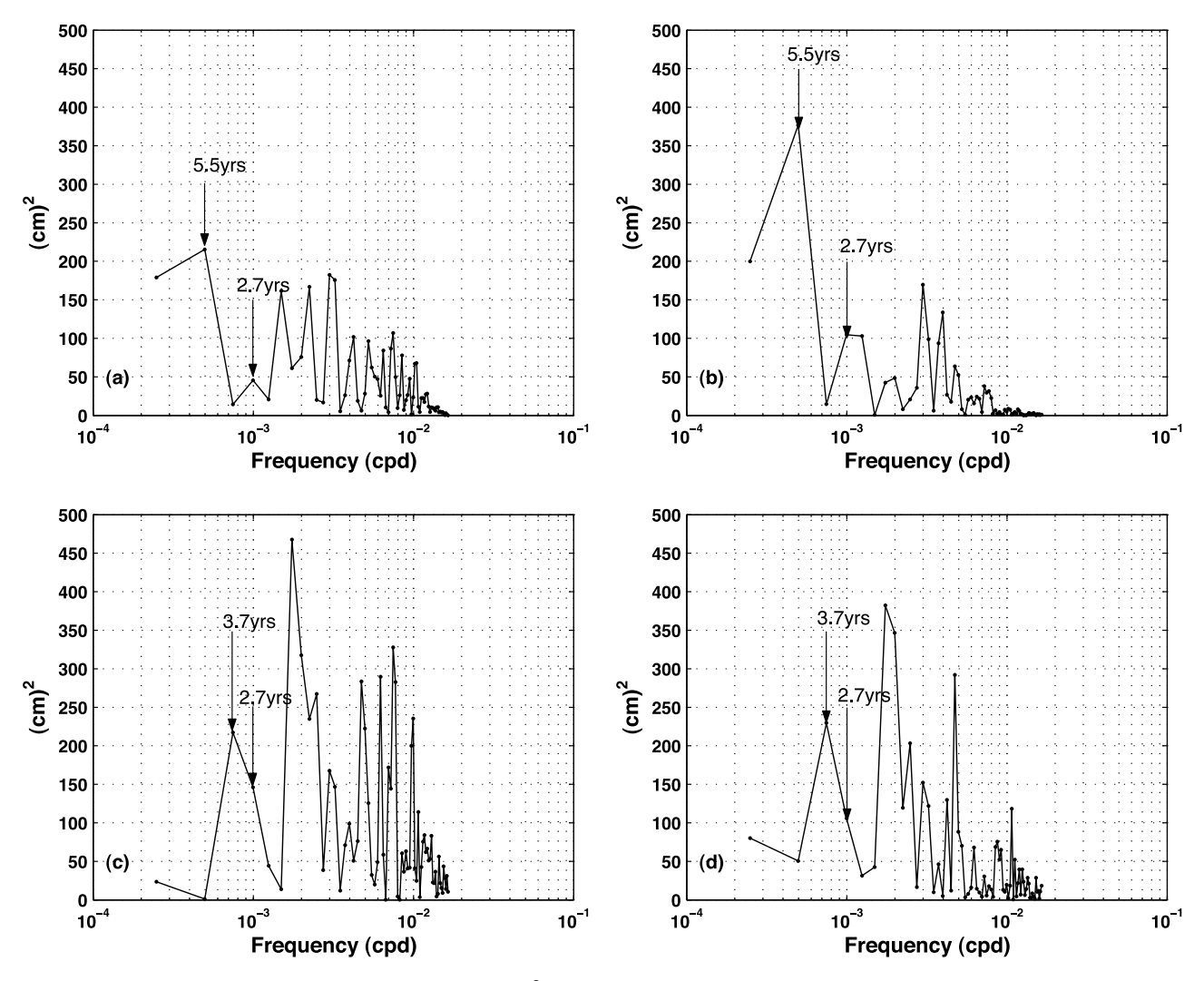


Figure 5. Variance preserving spectra (cm²) of dynamic height anomaly from (a, c) XBT data and (b, d) the POP model at the southern (Figures 5a and 5b) and northern (Figures 5c and 5d) ends of the IX1 transect.

over 90°W-150°W, 5°S-5°N) with that from data [Reynolds and Smith, 1994]. Very good agreement is seen (Figure 4a) from 1989-1998, except for 1994 through early 1995 when the model is too cold. In 1987 and 1988 the model index is in phase with the data, but underestimates the magnitude of the observed SSTA. This discrepancy is likely due to the adjustments made to the ECMWF reanalysis forcing fields to achieve a global balance on an annual basis; adjustments were larger in the 1980s relative to the very minor ones made in the 1990s. In all, the agreement is good (correlation between the two time series is 80%) giving us confidence to use the model to study interannual related variability in the Throughflow region.

[19] To better demonstrate the close phase agreement between Pacific El Niño and La Niña signals and the variability at the southern end of the IX1 transect, observed and modeled time series of the dynamic height anomalies were constructed by spatially averaging over the four most southerly bins (23.5°S–20.5°S). Dynamic height is used as it represents the variability over the upper water column. These time series are seen in Figure 4b together with the

equatorial SOI (EQSOI). The EQSOI was developed at the National Center for Environmental Prediction and is based on sea level pressures over Indonesia and the eastern equatorial Pacific [Kistler et al., 2001]. We use this index rather than the standard SOI, as we are interested in relating the remote equatorial and Northern Hemisphere off-equatorial ENSO signals that propagate through the Indonesian Seas to the variability at the southern end of IX1. The seasonal cycle has been removed from the EQSOI and a 5-month running mean has been applied to remove high-frequency fluctuations. All time series are normalized by their respective space-time standard deviations. Both time series are well correlated with the EQSOI: 0.58 for the observed time series, and 0.63 for the model time series. The correlation between the data and the model time series is 0.80. All relationships are significant at the 95% level. We note an unrealistically long La Niña is maintained by the model in 1989: both the EQSOI and the data time series start to decrease after peaking in early 1989, while the model values stay elevated until the end of the year. This is likely due to inaccuracies in the Pacific

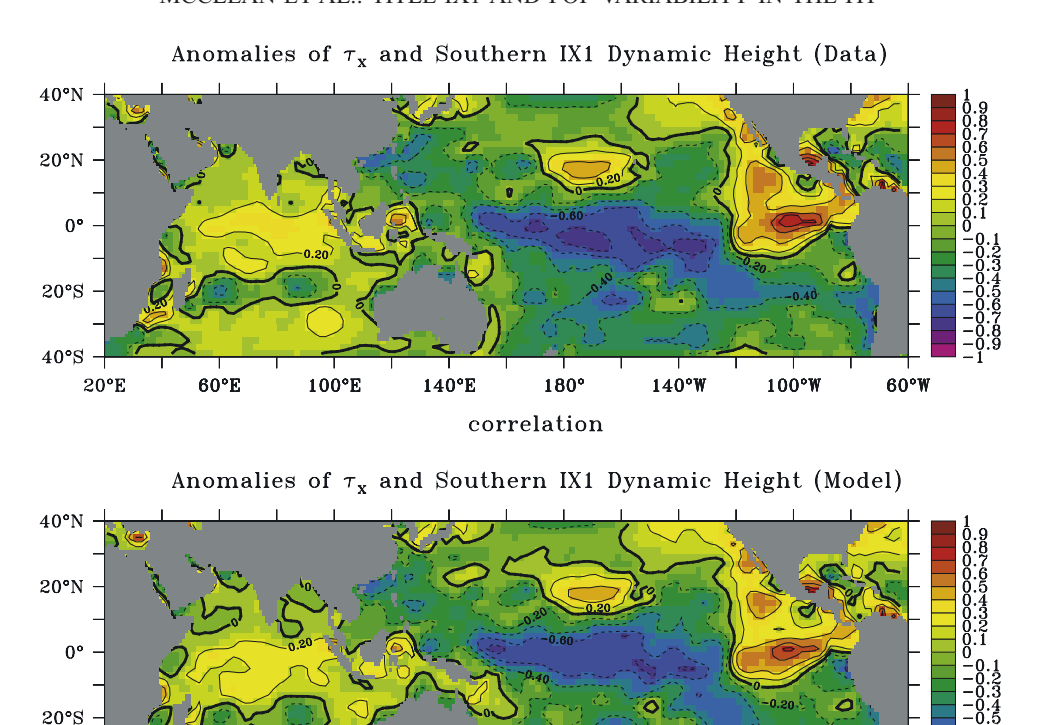


Figure 6. Correlations of dynamic height anomaly (cm) at the southern end of IX1 calculated from (top) IX1 data and (bottom) the POP model and zonal wind stress anomaly (dynes cm⁻²) over the tropical and midlatitudes of the Pacific and Indian oceans.

correlation

180°

140°W

100°W

60°W

140°E

surface forcing that resulted in an overly warm Pacific anomaly during the 1988 La Niña (Figure 4a).

60°E

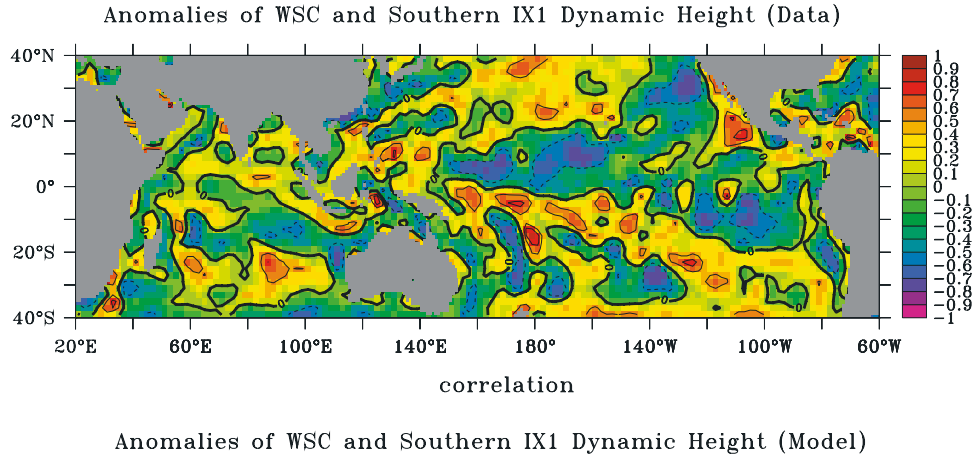
100°E

[20] Time series of the observed and modeled dynamic height anomaly from the northern end of the IX1 transect (8.5°S-9.5°S) are plotted along with the EQSOI and the Dipole Mode Index (DMI [Saji et al., 1999]) in Figure 4c. The seasonal cycle was removed from the DMI and it was low-pass filtered at 5 months. Clearly the data and model time series are visually inversely correlated with the DMI; both extreme dipole mode events in 1994 and 1997 are seen in the observed and modeled time series. Correlation values between the DMI and the data, and the DMI and the model, are -0.8 and -0.76, respectively. The correlation between the model and data is 0.84. All correlations are significant at the 95% level. Additionally, the observed and modeled time series are significantly correlated with the SOI index: values of 0.60 and 0.54 are obtained, respectively.

[21] To identify the dominant narrow-band periodicities, we calculated variance-preserving spectra of the data and model dynamic height anomaly time series from the northern and southern ends of the IX1 transect. Since our focus is on long-period signals, peaks with periodicities less than 1.8 years although present in the spectra are not discussed. The southern IX1 data and model spectra (Figures 5a and 5b) both display peaks at 2.7 and 5.5 years, with the magnitude of the 5.5-year signal being 4.7 (3.6) times larger than the observed (modeled) signal at 2.7 years. In addition, the modeled 5.5-year

signal is 1.7 times larger than the equivalent observed value. We refer to the 2.7 year signal as quasi-biennial (QB) and the 5.5 year as quasi-pentadal (QP). Clearly, the model is overestimating the strength of the 2.7 and 5.5-year signals, however in keeping with the observations, it does demonstrate that at the southern end of IX1, the QP variability is stronger than the QB signal. The spectra of the observed and modeled time series from northern IX1 (Figures 5c and 5d) display peaks at 3.7 years; the model peak (230 cm²) is just slightly larger than that of the data (215 cm²). Using variance-preserving spectra of averaged wind anomalies along the pathways of the equatorial and coastal waveguides from the Pacific and Indian oceans, Wijffels and Meyers [2004, Figure 11] found Pacific winds were dominated by ENSO (5-6 years) while the Indian Ocean winds displayed energy at around 3.3–3.7 years. Clearly, as shown in Figure 5, these Pacific and Indian Ocean remote signals are also contributing to the upper ocean response at the southern and northern ends of IX1, respectively.

[22] To further understand the nature of the remote signals impacting IX1 the zonal component of wind stress and the wind stress curl over the tropics and subtropics in the Indian and Pacific Oceans were correlated with the times series of dynamic height anomalies from the southern and northern ends of the IX1 transect. Both the model and the data time series were correlated with the ECMWF winds that were used to force the model. The seasonal cycle was removed from the winds, which were then low-



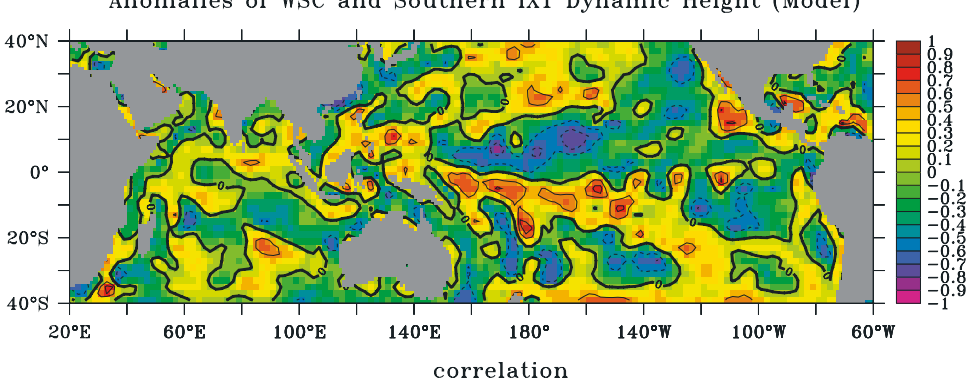


Figure 7. Correlations of dynamic height anomaly (cm) at the southern end of IX1 calculated from (top) IX1 data and (bottom) the POP model and wind stress curl anomaly (dynes cm⁻³) over the tropical and midlatitudes of the Pacific and Indian oceans.

pass filtered at 13 months, and interpolated to a $2^{\circ} \times 2^{\circ}$ grid. The IX1 model and data time series were also lowpass filtered at 13 months (capturing variability over interannual timescales). Figure 6, top and bottom plots, show the correlation between the zonal wind stress and the southern IX1 data and the model time series, respectively. Maximum negative correlations (≥ -0.70) for both time series were found with the equatorial winds over the western and central Pacific Ocean. The correlations were repeated using timescales greater than 3 years (QP), and correlation values increased to over -0.80, explaining about 70% of the variance. Maximum correlations between the northern IX1 time series and the zonal winds (not shown) occurred over the equatorial Indian Ocean; values greater than 0.8 were found on the equator between 80°E-90°E for both the model and the data. These findings indicate that remote signals generated along the equator in the Pacific and Indian oceans propagate along the equatorial and coastal waveguides into the IX1 region, consistent with the findings of Clarke and Liu [1994], M96, and Wijffels and Meyers [2004]. Correlations between the southern IX1 time series for both data and model and wind stress curl (low-pass filtered at 13 months) indicate that another remote oceanic signal is impacting this section of the transect (Figure 7). Maximum negative correlations (>-0.8) are seen between $\sim 5^{\circ}N$ and $10^{\circ}N$ in the western and central Pacific for both the model and the data. The relationship between variability at the southern end of IX1 and this remote off-equatorial signal in the Pacific will be

discussed in the next section in the light of the observational findings of White et al. [2003].

5. Discussion

[23] White et al. [2003] documented long period, offequatorial baroclinic Rossby waves in the Pacific basin with QB (2.2- and 2.8-year) and QP (3.5-, 5.4-, and 7-year) periodicities that propagate westward across the Pacific basin to arrive at the western boundary at approximately 7°N and 12°N, respectively. They argue that these offequatorial signals reach the western boundary of the Pacific and reflect as slow eastward propagating equatorial coupled waves. M96 and Wijffels and Meyers [2004] attributed the remote Pacific signal in their IX1 results to interannual free equatorial Rossby waves and reflected equatorial Kelvin waves whose energy radiates through the Indonesian Seas, as predicted by Clarke and Liu [1994]. M96 and Wijffels and Meyers [2004] did not discuss the impact of the offequatorial waves from the Pacific on the ITF region. In addition, the White et al. [2003], M96 and Wijffels and Meyers [2004] studies identified the waves using observational data sets. Here we investigate using the model, whose resolution and realistic topography resolve the waveguide through the Indonesian Seas, whether the remote signal found at the southern IX1 transect in Figure 7, can also be traced back to Pacific off-equatorial low-frequency Rossby waves. These waves would excite Kelvin-Munk waves at the western boundary of the Pacific, which in turn, would

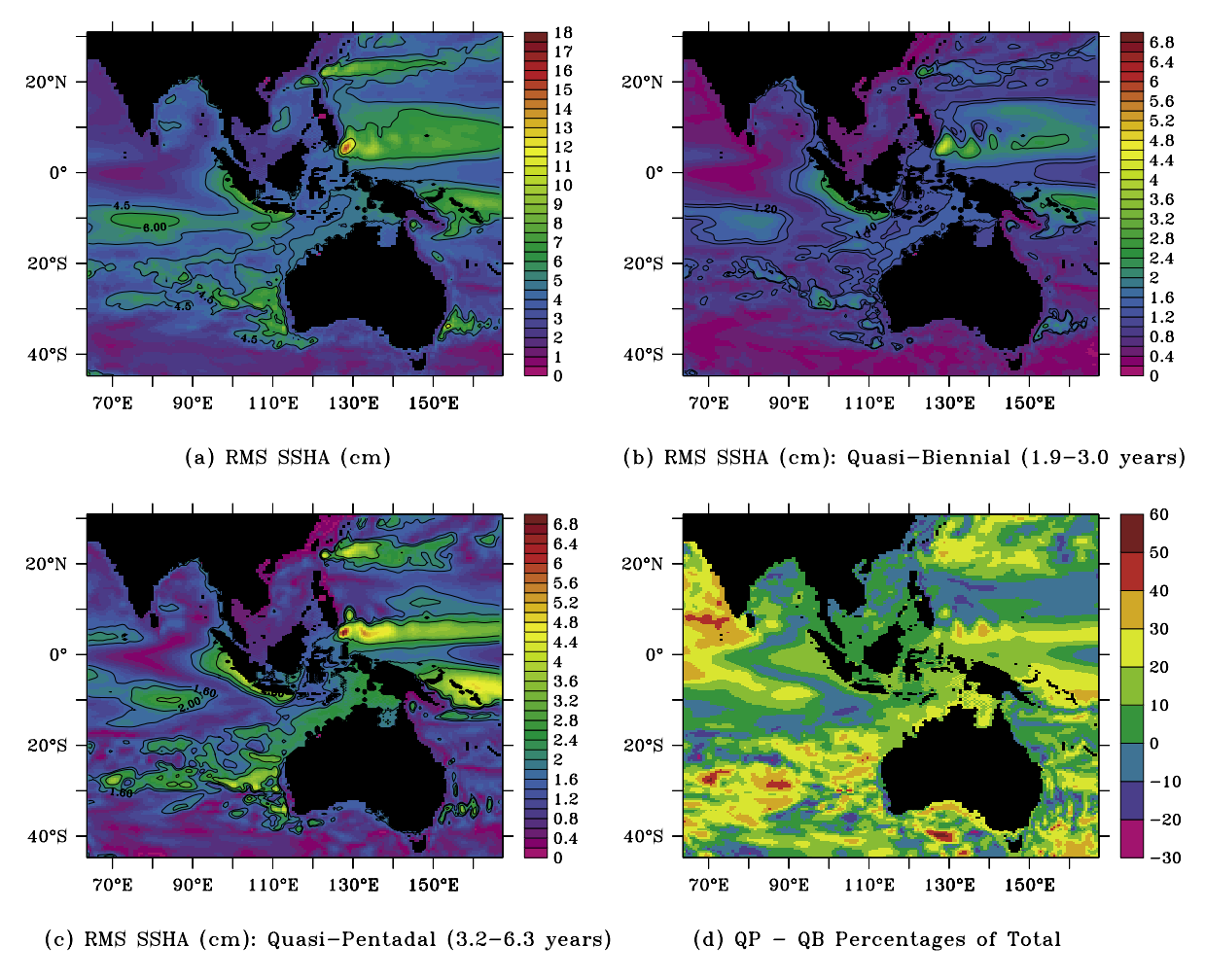


Figure 8. Root-mean square (RMS) of sea surface height anomaly (SSHA) in centimeters for (a) annual and semi-annual cycles removed and low-pass filtered at 4 months, (b) quasi-biennial band (1.9–3.0 years), (c) quasi-pentadal (3.2–6.3 years), and (d) quasi-pentadal—quasi-biennial percentages of total RMS SSHA as represented by Figure 8a, from POP for 1979–1997.

propagate equatorward to reflect as equatorial Kelvin waves, exciting a coastally trapped wave response that would propagate through the Indonesian Seas and along the northwest coast of Australia. This signal could then progressively propagate into the STIO as Rossby waves. We address the importance of both off-equatorial and equatorial long waves to the composition of the remote Pacific signal, and evaluate the penetration of this remote Pacific signal into the interior of the STIO.

[24] To understand the importance of the low-frequency signal in the tropical and sub-tropical western Pacific and eastern Indian Oceans, and the Indonesian seas, we calculated the root-mean square (RMS) of 3-day averages of sea surface height anomaly (SSHA) after first removing the annual and semi-annual cycles, detrending, and low-pass filtering at 4 months (Figure 8a). Sea surface height was chosen as it reflects variability in the upper water column. We used the entire length of the model run (1979–1997) to better resolve the QB and QP signals; 7 and 3.5 cycles were produced, respectively. Figure 8a clearly shows two zonal bands of high variability in the off-equatorial regions of the north and south Pacific. Relatively high RMS values are

also seen in the eastern channels of the Indonesian Seas, along the NW shelf of Australia, and between 5°S and 15°S in the Indian Ocean. Other regions of high RMS are found off Sumatra, around 20°N in the North Pacific, and to the south of 20°S in the Indian Ocean. This figure may be compared qualitatively to that obtained from altimeter data (0.25°grid) by Wijffels and Meyers [2004, Figure 16a], as the low-frequency signal of both the data and model was similarly isolated. Also, the model grid has latitudinal resolution of about 0.25° near the equator. Very good agreement is found between the model RMS SSHA (Figure 8a) and that from the altimeter data [Wijffels and Meyers, 2004] in terms of both distribution and magnitude of the variability. This good agreement provides a measure of the model integrity in this region and therefore gives us confidence in using it to understand the nature of the remote Pacific signal impacting the ITF.

[25] To appreciate the relative strengths of the variability in the narrow-band QB and QP bands, we band-pass filtered the SSHA in Figure 8a between 1.9–3 years (Figure 8b) and 3.2–6.3 years (Figure 8c), respectively. These periods correspond to the frequency range of separate peaks in an

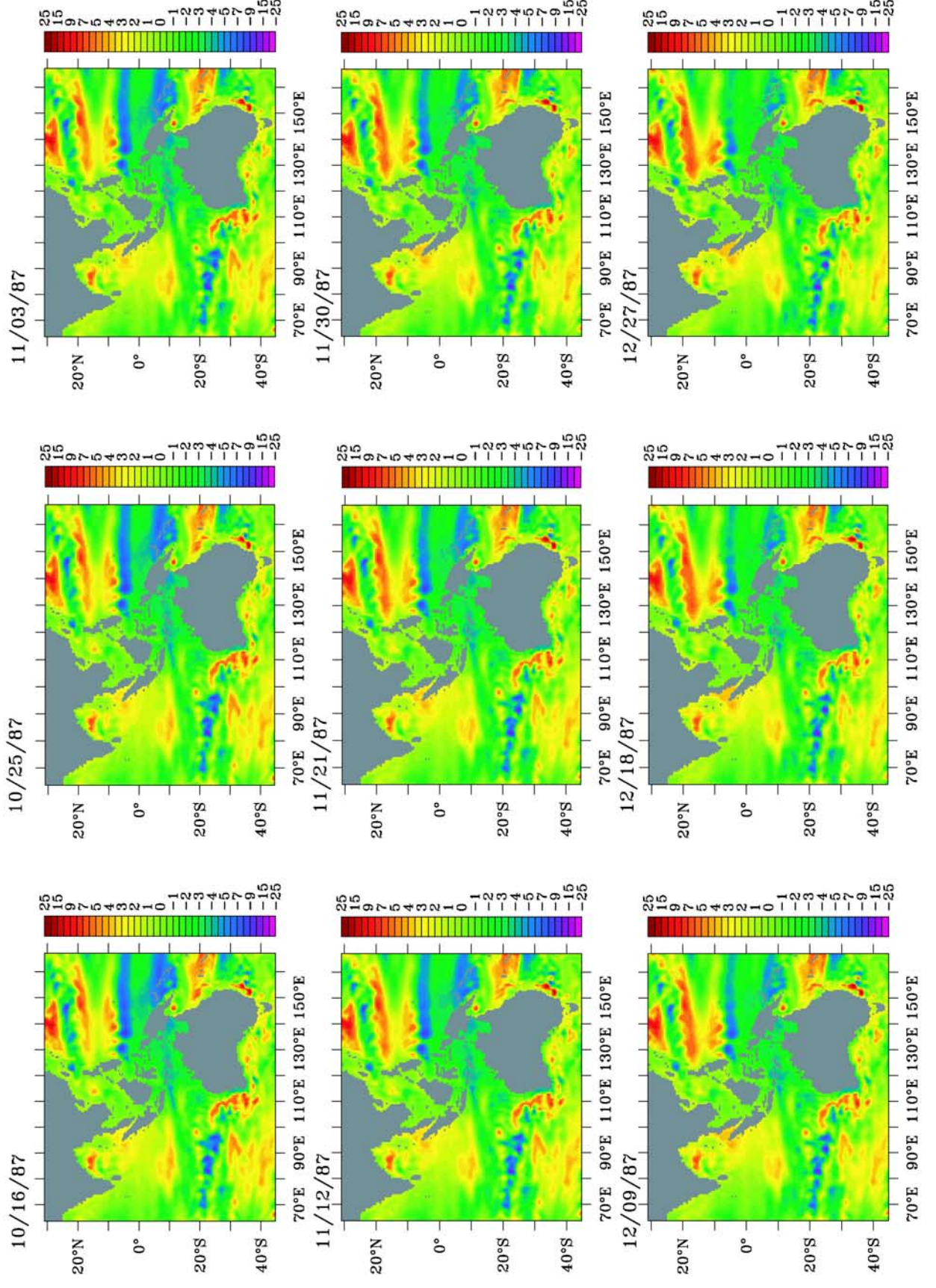


Figure 9. Time sequence of maps of SSHA (cm) for the period 16 October 1987 through 27 December 1987. SSHA was low-pass filtered at 13 months following the removal of the annual and semi-annual cycles.

area-averaged (90°E-°170°E, 20°S-20°N) variance-preserving spectrum of demeaned SSH (not shown). In both cases, the highest variability associated with each period is seen in the off-equatorial regions of the Pacific Ocean, the eastern channels of the Indonesian Seas, along the NW shelf of Australia, off Sumatra, and between 70°E and 90°E in the STIO. The percent of the total variability explained by each band was calculated and the QB percentage was then subtracted from the QP variability (Figure 8d). In the regions where the highest variability was observed in Figures 8b and 8c, the QP band is roughly 10-25% more energetic than the QB band. This agrees with the stronger QP signal compared to the QB signal in the variance-preserving spectra of the southern IX1 shown in Figure 5. As a result in the following event analyses we will not attempt to separate out the QB and QP signals, rather we will consider their combined effects as an overall "interannual" signal.

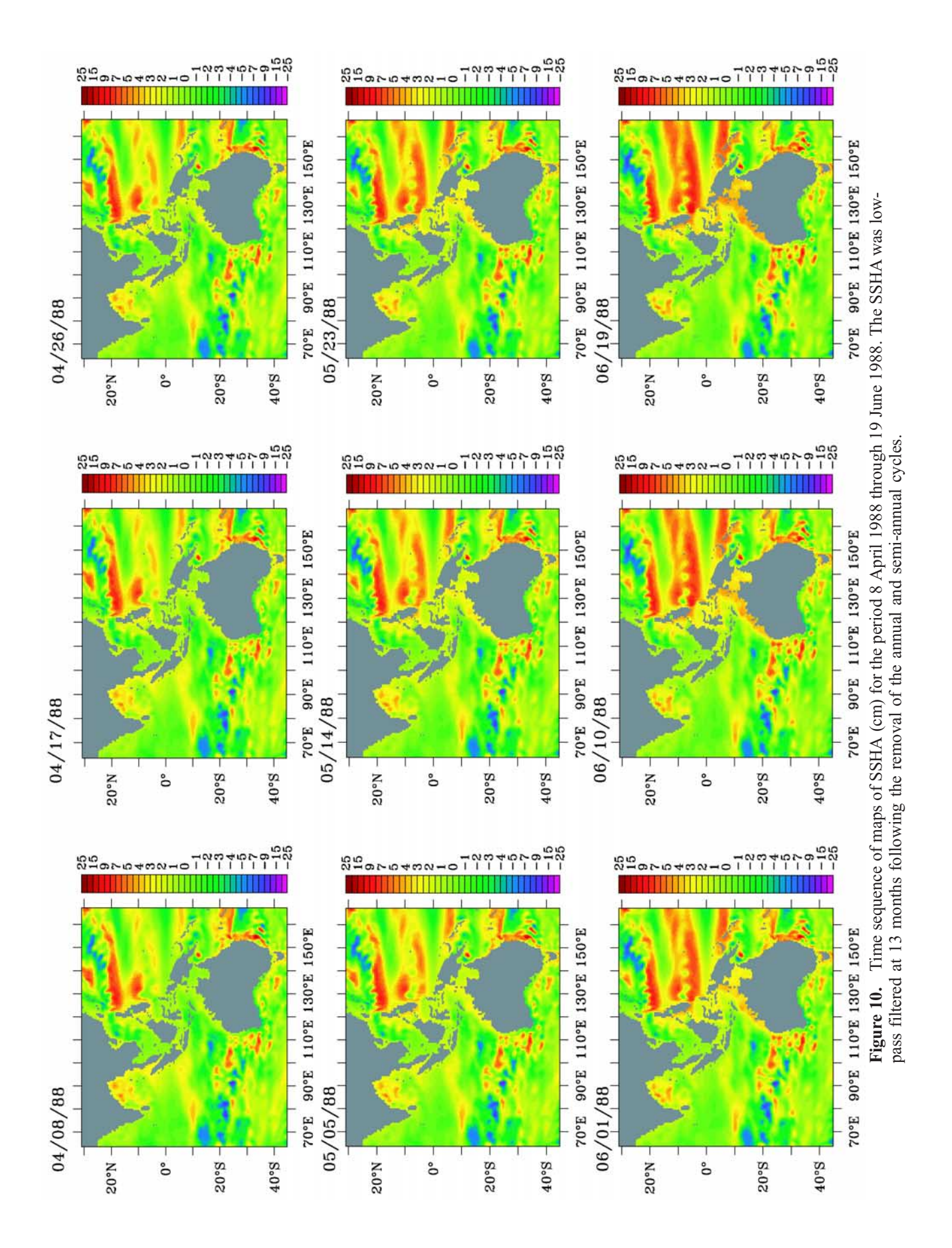
[26] To help distinguish between the off-equatorial and the equatorial pathways, and to understand the changes in the space-time structure of these low-frequency signals passing through the Indonesian Seas from the North Pacific, we show two time series of snapshots of SSHA: one depicting the passage of equatorial Rossby waves and the other the evolution of the off-equatorial signal. These snapshots were derived from an animation of the full time series (1979–1997). Annual and semi-annual cycles were first removed from the demeaned SSH by least squares fitting; it was then detrended and low-pass filtered at 13 months (to include all QB and QP frequencies).

[27] Figure 9 shows the low-frequency signal during the 1987 El Niño for the period 16 October 1987 through 27 December 1987. The equatorial Rossby wave can be easily recognized by the band of negative SSHA spanning the equator with its maximum amplitude occurring at about 5° in both hemispheres. Negative anomalies are seen throughout the Indonesian Seas and along the NW shelf of Australia. By 27 December 1987, the wave has diminished in magnitude. We move forward to 8 April 1988 (Figure 10) and now see negative SSHA on the equator associated with Kelvin wave activity (from the reflected equatorial Rossby wave), while positive SSHA signals are increasing in magnitude in the off-equatorial regions. Focusing on the northern hemisphere, we see a combination of processes underway. A band of intensifying positive SSHA (8 April 1988 to 14 May 1998 and onward) is seen between the northern tip of Halmahera Island extending northwestward to about 170°E, 8°N. A Hovmueller (time versus longitude) diagram (not shown) depicts westward propagating waves entering this region from the east between 6°N and 9°N; however, to the west of 150°E the signal is also due to local wind stress curl anomalies (see Figure 7). Concurrently, intensifying positive SSHA is found along the Irian Jaya shelf, in the Arafura/Australian waveguide, and along the NW Australian shelf. Near 10°N-12°N a positive SSHA signal is seen at 160°E on 8 April 1988. It can be seen at progressively more westward locations at subsequent dates, until by 19 June 1988, a continuous band of positive SSHA is found across 10°N-12°N. A Hovmueller plot along this latitude band (not shown) indeed confirmed this to be a westward propagating wave. Increasingly positive SSHA is also seen spreading westward in the Banda Sea. Subsequent

SSHA snapshots show the signal to further intensify over the entire region and to progress eastward along the equator, indicative of reflection at the western boundary. Along the NW Australian shelf, the signal is seen to propagate offshore. In the southern hemisphere, positive SSHA is seen between 5°S and 8°S east of New Guinea (Figure 10). Tracking the signal in the time sequence ending 19 June 1988, it is seen to intensify at this location, however only a very weak positive SSHA signal is seen closer to the equator to the north of New Guinea. The local coastal waveguide here intersects the equator to the east of the northern tip of Irian Jaya which itself extends north of the equator. It appears from the animation (later time, not shown) that this weak off-equatorial signal on reaching the equator reflects to the east of Irian Jaya and is therefore unlikely to impact the Indonesian Seas.

[28] This scenario described by Figure 10 is in agreement with White et al. [2003]: Low-frequency westward propagating baroclinic Rossby waves are found in the offequatorial western Pacific following the warm phase of ENSO. White et al. [2003] were able to track the incident paths of these low-frequency off-equatorial Rossby waves at the northwestern Pacific boundary and their emergence along the equatorial Pacific as coupled waves. They did not, however, track these signals through the ITF. We contend that upon reflecting onto the equator, the resulting coupled waves excite a coastally trapped response in the Indonesian Seas that propagates along the NW shelf of Australia. To further understand the relationship between the remote Pacific signals and the STIO where the QP variability appears to be strongest (Figure 8c), we use crossspectral analyses (coherence-squared and phase calculations) of 3-daily SSHA (demeaned only) between the southern end of the IX1 line (110°E, 22°S) and each grid point of the model domain in the STIO and the western tropical Pacific. The autospectral density functions, the co-spectrum and the quadrature spectrum calculated as part of the coherence-squared/phase calculation were averaged over three adjacent frequency bands to produce 6 degrees of freedom. The demeaned SSH were pre-whitened using a finite difference filter prior to calculating the spectra. Only the OP frequency bands are selected and discussed here as the QB signals have already been shown to be of lesser importance particularly off western Australia (Figure 5). The coherence-squared between SSHA at 110°E, 22°S (identified by a star) and the SSHA at other grid points in the domain for the QP frequencies are seen in the top panel of Figure 11a. Regions where the coherence-squared is below the 90% significance level (0.69) are shaded gray. The 95% significance level is 0.78. The middle panels show the equivalent phase, with its associated error in the bottom panels, between each pair in the time series.

[29] Statistically significant coherence-squared values are seen in the tropical North Pacific between 150°E and the maritime western boundary as far north as 15°N (Figure 11a). The highest values (>0.9) in this region are seen off the equator (7°N–8°N). Significant values are found in the Halmahera, Seram, and Banda Seas, in Ombai Strait, and along and offshore of the NW Australian shelf to the south of Timor Strait (see Figure 1 for locations). The negative phases in the Indonesian Seas and in the western Pacific associated with these coherence-squared values



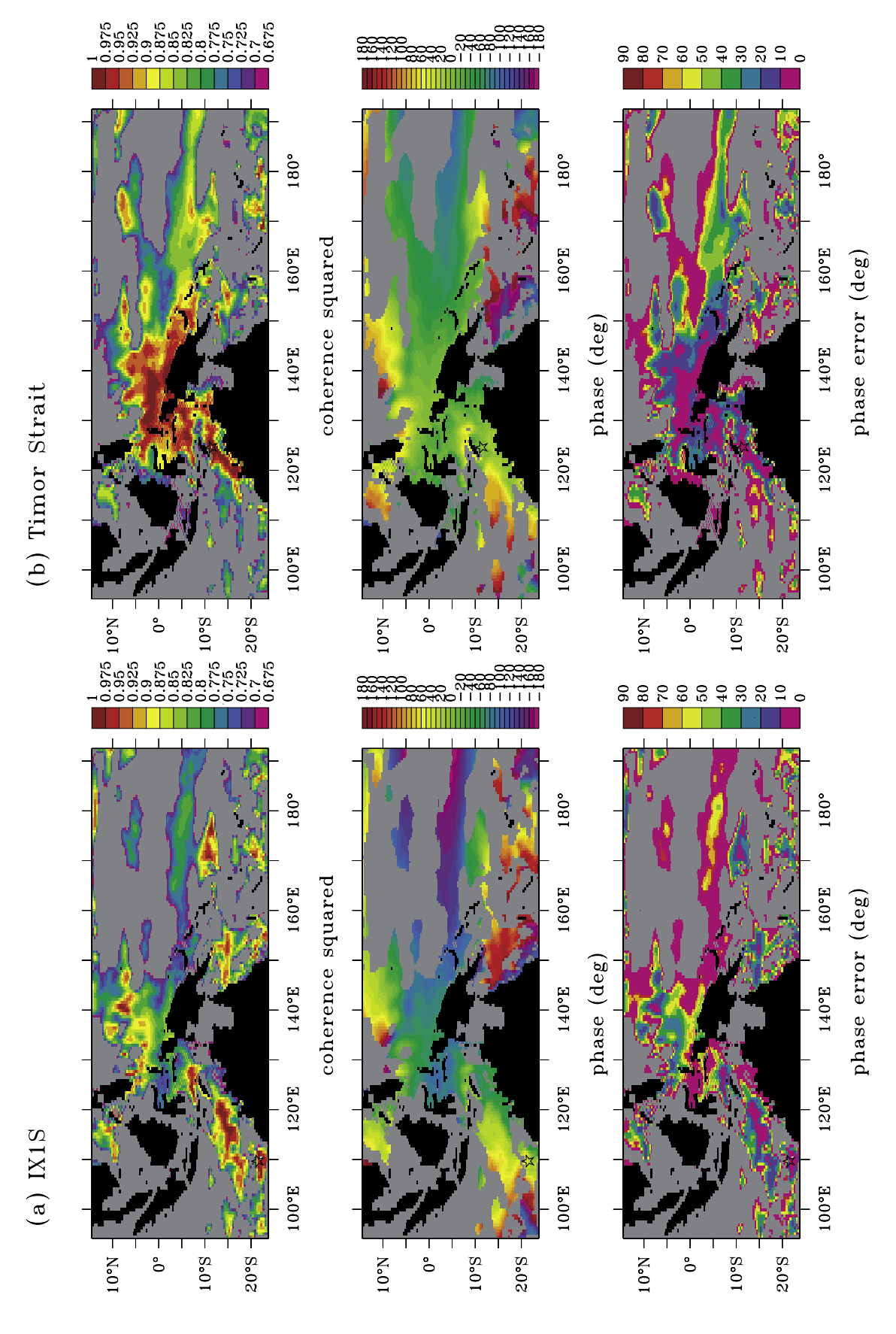


Figure 11. Cross-spectrum of SSHA at quasi-pentadal frequencies between each grid point of the model domain in the (b) Timor Strait (125°E, 12°S); these locations are identified by stars. (top) Coherence-squared values (areas shaded gray are below the 90% significance level) AND (middle) phases with (bottom) their associated error. southern tropical Indian Ocean and the western tropical Pacific and (a) the southern end of the IX1 line (110°E, 22°S) and

indicate that the SSHA at the southern end of the IX1 line lags the SSHA at these locations. Positive phases in the western Pacific to the north of $8^{\circ}N$ are consistent with the arrival of the Rossby waves at $10^{\circ}N-12^{\circ}N$ after the lower latitude signals in the western Pacific have started to penetrate and impact the STIO, as seen in Figure 10. The positive phases to the north and to the west of $110^{\circ}E, 22^{\circ}S$ indicate that the signal that radiates offshore of Australia is lagging that at the southern end of IX1. The phase error is up to $\pm 20^{\circ}where$ the coherence-squared values are $>\!0.9$.

[30] These analyses strongly suggest that for QP periodicities the southern IX1 line is affected by signals originating in both the equatorial and off-equatorial northwestern tropical Pacific. Coastally trapped responses are generated by either equatorial Rossby or reflected Kelvin waves resulting from the Munk-Kelvin waves or the equatorial Rossby waves. The signals propagate southwards through the Halmahera Sea into the Seram Sea and then southwestward around the Banda Sea to pass through Ombai Strait, A visual correlation of the 1000-m isobath in the Indonesian Seas (Figure 1) and the pathway of the coherent signal around the Banda Sea and southwestward along the NW Australian shelf shows that the signal is propagating along the continental shelf. The signal finally radiates offshore as a Rossby wave into the STIO. A statistically significant signal does not exist west of 90°E, in agreement with earlier observational findings by Masumoto and Meyers [1998]. Using OGCM output and XBT data, they found that interannual variations of the D_{20} in this region were largely due to the wind stress curl integrated along the Rossby wave pathways. However, in their models, both Murtugudde et al. [2000] and Xie et al. [2002] suggested that during El Niño periods, there is significant SST variability in the western STIO that can be linked to these Rossby waves generated in the eastern STIO.

[31] The results shown in Figure 11a can be contrasted with those obtained by calculating cross-spectra of SSHA between a location in Timor Strait (125°E, 12°S, again identified by a star) and the rest of the domain for QP frequencies (Figure 11b). Statistically significant coherence is again seen in the western tropical Pacific, however values are slightly lower to the north of 8°N than in Figure 11a. Patches of high coherence-squared values (>0.95) are seen close to the equator from 140°E to Halmahera in the northern hemisphere and north of Irian-Jaya in the southern hemisphere, in the Seram, Banda, and Arafura Seas, and on the NW Australian shelf to about 17°S. Westward propagating wave crests are found along the Pacific equator in the associated phase diagram (middle panel); here the phase is progressively less negative as the western boundary is approached. In the Indonesian Seas and on the NW Australian shelf the phase is unchanged. Clearly, the Timor Strait SSHA is most strongly correlated with the equatorial Pacific signal.

[32] It has been demonstrated from all these model analyses that the STIO is impacted by both remote Pacific equatorial and off-equatorial Rossby waves. Using XBT data, *Wijffels and Meyers* [2004] clearly found equatorial Pacific winds to be driving the interannual temperature and sea level response as represented by free equatorial Pacific Rossby waves. The signal radiated

through the Banda Sea into the STIO as well as entering the coastal waveguide at the western tip of New Guinea and propagating poleward through Timor Strait and along the Arafura/Australian shelf break as coastally trapped waves. In turn, these trapped waves excited free westward propagating Rossby waves that could be detected several hundreds of kilometers offshore at 22°S. The model, as shown in Figure 11, reproduced all these wave processes. As well, the model delineates an off-equatorial North Pacific signal that enters the coastal waveguide and propagates southward through the Halmahera Sea into the Seram Sea and then southwestward around the Banda Sea to pass through Ombai Strait. These off-equatorial waves form in response to off-equatorial cyclonic wind stress curl anomalies (Figure 7), induced by westerly surface wind anomalies produced in the wake of warm SST anomalies that propagate slowly eastward along the equator [White et al., 2003]. Interestingly, the low-frequency lagged regressions of Wijffels and Meyers [2004, Figure 17a] also revealed a strong response in offequatorial western Pacific sea level anomaly to Pacific easterly equatorial wind anomalies. This suggests that the off-equatorial signal passing through the ITF and reaching the STIO, as demonstrated by the model, also occurs in reality. Wijffels and Meyers [2004] did not look for or identify this pathway in their observational study.

[33] Clearly, the remotely forced long waves interacting with the complex topography of the Indonesian Throughflow produce varied responses in different parts of the STIO. For completeness, we also computed cross-spectra of SSHA at OP frequencies between points in the northern and middle part of the IX1-XBT line and the rest of the domain to help identify other possible remote influences (figures not shown). For locations at the northern end of the IX1-XBT line, a significant coherent, in-phase signal in SSHA was evident off the coast of Sumatra and Java, extending through the Lombok Strait into Makassar Strait: the coherence drops off to the north of the Dewakang sill at 2°S in Makassar Strait. This signal is likely due to interannual Kelvin waves forced remotely by equatorial interannual zonal winds in the Indian Ocean as discussed by Clarke and Liu [1994] and Wijffels and Meyers [2004]. For locations in the middle of the IX1-XBT transect (15°S-19°S), significant coherence is only found offshore of the NW Australian shelf in the STIO. Here the negative phases to the east and positive phases to the west of the IX1 line indicate the signal is due to Rossby waves propagating away from the west Australian coast.

6. Conclusions

[34] The mean and interannual variability of the thermal structure of the repeat XBT line known as IX1 were compared statistically for the years 1987–1997 with concurrent, co-located output from a global eddy-permitting configuration of the POP model forced with realistic surface fluxes. Both data and the model showed that the QP signal was strongest at the southern end of the IX1 line where it exhibited variability nearly in phase with ENSO in the Pacific. The dominant low-frequency variability (3.7 years) at the northern end of IX1 was attributed to remote forcing from the equatorial Indian Ocean. Correlations between the

observed and model time series and the winds in both the tropical and subtropical Indian and Pacific oceans further confirmed this result.

[35] The model demonstrated integrity in its representation of low-frequency variability as demonstrated by comparisons with data analyses presented in this study, and with results from previous observational studies. In particular, the data/model comparisons of dynamic height variability at the southern and northern ends of IX1 and the comparison of RMS SSHA from altimetry [from Wijffels and Mevers, 2004] and the model in the Indo-Pacific domain showed strong agreement. Model discrepancies such as the remote Pacific signal being too strong and lasting for too long in the model STIO are likely due to shortcomings in the surface forcing over the Pacific, particularly the annual adjustment over the tropics to balance the global heat balance. The SST discrepancy in the STIO may also be due to inaccuracies in the surface forcing and other factors such as the lack of tidal mixing in the model.

[36] White et al. [2003] stated that low-frequency Rossby waves form in response to off-equatorial cyclonic wind stress curl anomalies induced by westerly surface wind anomalies produced in the wake of warm SST anomalies that propagate slowly eastward along the equator. In our study, we found that off-equatorial Rossby waves, on reaching the western maritime boundary of the North Pacific, excited a coastally trapped response (Munk-Kelvin waves) that propagated equatorward and reflected onto the equator. In turn, this equatorial signal excited a coastally trapped response off Irian Jaya that propagated through the Indonesian Seas and along the northwest coast of Australia where it progressively radiated off as Rossby waves into the STIO. Cross-spectral analyses confirmed that on QP scales, the free westward propagating Rossby waves in the STIO excited by coastally trapped waves along the NW shelf, resulted from both equatorial and off-equatorial lowfrequency signals remotely forced in the Pacific Ocean. Comparative cross-spectral analyses, suggested that Timor Strait is more strongly affected by the equatorial signal than the off-equatorial signal, while the southern IX1 responds to both.

[37] The northern end of the IX1 XBT transect responded to interannual Kelvin waves forced remotely by equatorial interannual zonal winds in the Indian Ocean as discussed by Clarke and Liu [1994], while the middle of the transect only experienced the passage of Rossby waves propagating away from the west Australian coast. In the POP model used here, these Rossby waves do not penetrate farther westward than 90°E as found by Masumoto and Meyers [1998]. These results further attest to the integrity of the simulation and hence the reliability of the model findings that have not been identified from data. Clearly, the resolution and realistic topography of the model has allowed us to resolve the waveguide through the Indonesian Seas and understand the varied responses on low-frequency timescales in the STIO to remotely forced long waves.

[38] A study of the energy transmission and the transport variability associated with the passage of these coastally trapped waves through the Indonesian Seas and along the NW Australian shelf would further quantify the importance of these signals to the STIO. However, these calculations

would be better performed with a higher resolution model that will more accurately depict the complex bathymetry of the region. A suitable candidate is the 0.1°, 40-level global POP simulation [Maltrud and McClean, 2005]; some 2 decades of a spin-up integration have recently been completed and a post spin-up simulation is now underway.

[39] **Acknowledgments.** The Department of Energy (CCPP program) and the National Science Foundation (OCE-0221781 (J. M.) and OCE-0220382 (J. S.)) sponsored this work. The Alaska Region Supercomputing Center (ARSC) provided computer time. We thank Susan Wijffels and Gary Meyers (CSIRO, Australia) for the IX1-XBT data. We thank Tony Craig (NCAR) and Wieslaw Maslowksi (NPS) for collaborating with the authors to set up and test the global POP simulation. Mathew Maltrud (LANL) provided the global model grid. Robin Tokmakian (NPS) collaborated with the authors in the processing of the ECMWF reanalysis fluxes. Peter Braccio performed some of the post-processing of the model output. We obtained the Indian Ocean Dipole Mode Index from Kevin Vranes (http:// www.ldeo.columbia.edu/~kvranes/research/DMI). The NINO3 data was obtained from the IRI/LDEO Climate data library (http://ingrid.ldeo. columbia.edu). We thank Jim Potemra and Ted Durland (U. Hawaii) for comments on an earlier draft. The reviewers and editors are thanked for their helpful comments.

References

Behera, S. K., P. S. Salvekar, and T. Yamagata (2000), Simulation of Interannual SST variability in the tropical Indian Ocean, *J. Clim.*, 13, 3487–3499.

Böning, C. W., and R. G. Budich (1992), Eddy dynamics in a primitive equation model: Sensitivity to horizontal resolution and friction, *J. Phys. Oceanogr.*, 22, 361–381.

Bryden, H. L., and S. Imawaki (2001), Ocean transport of heat, in *Ocean Circulation and Climate*, edited by G. Siedler, J. Church, and J. Gould, pp. 445–474, Elsevier, New York.

Clarke, A. J., and X. Liu (1994), Interannual sea level in the northern and eastern Indian Ocean, *J. Phys. Oceanogr.*, 24, 1224–1235.

Dukowicz, J. K., and R. D. Smith (1994), Implicit free-surface method for Bryan-Cox-Semtner ocean model, *J. Geophys. Res.*, 99, 7991–8014

Ffield, A., and A. Gordon (1996), Tidal mixing signatures in the Indonesian Seas, *J. Phys. Oceanogr.*, 26, 1924–1937.

Godfrey, J. S. (1975), On ocean spindown: I. A linear experiment, J. Phys. Oceanogr., 5, 399–409.

Godfrey, J. S. (1996), The effect of the Indonesian Throughflow on ocean circulation and heat exchange with the atmosphere: A review, *J. Geophys. Res.*, 101, 12,217–12,237.

Gordon, A. L. (2001), Interocean exchange, in *Ocean Circulation and Climate*, edited by G. Siedler, J. Church, and J. Gould, chap. 4.7, pp. 303–314, Elsevier, New York.

Jakob, C. (1999), Cloud cover in the ECMWF Reanalysis, J. Clim., 12, 947–959.

Kistler, R., et al. (2001), The NCEP-NCAR 50-year reanalysis: Monthly means CD-ROM and documentation, *Bull. Am. Meteorol. Soc.*, 82, 247-268.

Large, W. G., J. C. McWilliams, and S. C. Doney (1994), Oceanic vertical mixing: A review and a model with a nonlocal boundary layer parameterization, *Rev. Geophys.*, 32, 363–403.

Levitus, S., R. Burgett, and T. P. Boyer (1994a), *World Ocean Atlas 1994*, vol. 3, *Salinity, NOAA Atlas NESDIS 3*, Natl. Oceanic and Atmos. Admin., Silver Spring, Md.

Levitus, S., R. Burgett, and T. P. Boyer (1994b), *World Ocean Atlas 1994*, vol. 4, *Temperature, NOAA Atlas NESDIS 4*, Natl. Oceanic and Atmos. Admin., Silver Spring, Md.

Lukas, R., T. Yamagata, and J. P. McCreary (1996), Pacific low-latitude western boundary currents and the Indonesian Throughflow, *J. Geophys. Res.*, 101, 12,209–12,216.

Maltrud, M. E., and J. L. McClean (2005), An eddy resolving global 1/10° ocean simulation, *Ocean Modell.*, 8, 31–54.

Masumoto, Y. (2002), Effects of interannual variability in the eastern Indian Ocean on the Indonesian Throughflow, *J. Oceanogr.*, 58, 175–182.

Masumoto, Y., and G. Meyers (1998), Forced Rossby waves in the southern tropical Indian Ocean, *J. Geophys. Res.*, 103, 27,589–27,602.

McCreary, J. P. (1983), A model of tropical ocean-atmosphere interaction, Mon. Weather Rev., 111, 370–387.

Meyers, G. (1996), Variation of Indonesian Throughflow and the El Niño—Southern Oscillation, *J. Geophys. Res.*, 101, 12,255–12,263.

- Meyers, G., R. J. Bailey, and A. P. Worby (1995), Geostrophic transport of Indonesian Throughflow, *Deep Sea Res.*, *Part I*, 42, 1163–1174.
- Morrow, R., and F. Birol (1998), Variability in the southeast Indian Ocean from altimetry: Forcing mechanisms for the Leeuwin Current, *J. Geo*phys. Res., 103, 18,529–18,544.
- Murtugudde, R., J. P. McCreary, and A. J. Busalacchi (2000), Oceanic processes associated with anomalous events in the Indian Ocean with relevance to 1997–1998, *J. Geophys. Res.*, 105, 3295–3306.
- Pazan, S. E., W. B. White, M. Inoue, and J. J. O'Brien (1986), Off-equatorial influence upon Pacific equatorial dynamic height variability during the 1982–1983 El Niño–Southern Oscillation event, *J. Geophys. Res.*, 91, 8437–8450.
- Perry, G. D., P. B. Duffy, and N. L. Miller (1996), An extended data set of river discharges for validation of the general circulation models, *J. Geo*phys. Res., 101, 21,339–21,349.
- Philander, S. G. (1990), El Niño, La Niña and the Southern Oscillation, 293 pp., Elsevier, New York.
- Potemra, J. T. (1999), Seasonal variations of upper ocean transport from the Pacific to the Indian Ocean via Indonesian Straits, J. Phys. Oceanogr., 29, 2930–2944.
- Quadfasel, D., and G. Cresswell (1992), A note on the seasonal variability of the South Java Current, J. Geophys. Res., 97, 3685–3688.
- Reynolds, R. W., and T. M. Smith (1994), Improved global sea surface temperature analyses, *J. Clim.*, 7, 929–948.
- Saji, N. H., B. N. Goswami, P. N. Vinayachandran, and T. Yamagata (1999), A dipole mode in the tropical Indian Ocean, *Nature*, 401, 360–363.
- Schiller, A., J. S. Godfrey, P. C. McIntosh, G. Meyers, and R. Fiedler (2000), Interannual dynamics and thermodynamics of the Indo-Pacific Oceans, J. Phys. Oceanogr., 30, 987–1011.
- Smith, W. H. F., and D. T. Sandwell (1997), Global seafloor topography from satellite altimetry and ship depth soundings, *Science*, 277, 1957– 1962.
- Sprintall, J., J. Chong, F. Syamsudin, W. Morawitz, S. Hautala, N. Bray, and S. Wijffels (1999), Dynamics of the South Java Current in the Indo-Australian basin, *Geophys. Res. Lett.*, 26, 2493–2496.
- Sprintall, J., S. Wijffels, T. Chereskin, and N. Bray (2002), The JADE and WOCE 110/IR6 Throughflow sections in the southeast Indian

- Ocean: Part 2. Velocity and transports, *Deep Sea Res., Part II*, 49, 1363-1390.
- Wajsowicz, R. C. (1996), The response of the Indo-Pacific Throughflow to interannual variations in the Pacific wind stress: Part II. Realistic geometry and ECMWF wind stress anomalies for 1985–89, *J. Phys. Oceanogr.*, 26, 2589–2610.
- Washington, W. M., et al. (2000), Parallel climate model (PCM) control and transient simulations, *Clim. Dyn.*, 16, 755–774.
- White, W. B., Y. He, and S. E. Pazan (1989), Off-equatorial westward propagating Rossby waves in the tropical Pacific during the 1982–1983 and 1986–87 ENSO events, *J. Phys. Oceanogr.*, 19, 1397–1406.
- White, W. B., Y. M. Tourre, M. Barlow, and M. Dettinger (2003), A delayed action oscillator shared by biennial, interannual, and decadal signals in the Pacific Basin, *J. Geophys. Res.*, 108(C3), 3070, doi:10.1029/2002JC001490.
- Wijffels, S., and G. Meyers (2004), An intersection of oceanic waveguides: Variability in the Indonesian Throughflow region, *J. Phys. Oceanogr.*, *34*, 1232–1253.
- Wijffels, S., J. Toole, and R. Davis (2001), Revisiting the South Pacific subtropical circulation: A synthesis of World Ocean Circulation Experiment observations along 32°S, *J. Geophys. Res.*, 106, 19,481–19,514.
- Wijffels, S., J. Sprintall, M. Fieux, and N. Bray (2002), The JADE and WOCE I10/IR6 Throughflow sections in the southeast Indian Ocean: Part 1: Water mass distribution and variability, *Deep Sea Res.*, *Part II*, 49, 1411–1422.
- Yamagata, T., K. Mizuno, and Y. Masumoto (1996), Seasonal variations in the equatorial Indian Ocean and their impact on the Lombok Throughflow, *J. Geophys. Res.*, 101, 12,465–12,473.
- Xie, S.-P., H. Annamalai, F. A. Schott, and J. P. McCreary (2002), Structure and mechanisms of South Indian Ocean climate variability, *J. Clim.*, 15, 864–878.

D. P. Ivanova, J. L. McClean, and J. Sprintall, Scripps Institution of Oceanography, University of California, San Diego, La Jolla, CA 92093-0230, USA. (jmcclean@ucsd.edu)